Metabolic stress-induced phosphorylation of KAP1 Ser473 blocks mitochondrial fusion in breast cancer cells

Chun-Ting Cheng[1,2], Ching-Ying Kuo[1], Ching Ouyang[3], Chien-Feng Li[4,5], Yiying Chung[1], David C. Chan[6], Hsing-Jien Kung[7,8] and David K. Ann[1,2*]

Running title: pS473-KAP1 regulates mitochondrial dynamics

Keywords: breast cancer, KAP1 Ser473-phosphorylation, MFN2, metabolic stress

[1] Diabetes & Metabolism Research Institute, [2] Irell & Manella Graduate School of Biological Sciences, [3] Department of Molecular Medicine, Beckman Research Institute, City of Hope, Duarte, CA 91010, USA

[4] Department of Pathology, Chi-Mei Medical Center, Tainan, Taiwan

[5] Department of Biotechnology, Southern Taiwan University of Science and Technology, Tainan, Taiwan

[6] Department of Biology and Biological Engineering, California Institute of Technology, Pasadena, CA 91125, USA

[7] Department of Biochemistry & Molecular Medicine, UC Davis Comprehensive Cancer Center, Sacramento, CA 95817, USA

[8] National Health Research Institutes, Miaoli, Taiwan

Financial Support

National Institute of Health Research Grants R01DE10742, R01DE14183 and The Mary Kay Foundation Research Grant number 005-13 (to D.K.A.), and Ministry of Health and Welfare Research Grant MOHW103-TD-M-111-102001 (to C.F.L.), and R01CA165263, R01CA150197, MOHW104-TDU-M-212-13304, MOST102-2320-B-400-018-MY3, MOST104-2321-B-400-009 and NHRI05A1-MGPP15-014 (to H.J.K.) and P30CA33572.

Conflict of Interest

The authors declare that they have no conflict of interest.

Word Count: 5540
Figure number: 6
Table number: 1
Movie: 4

* To whom all correspondence should be addressed:

David K. Ann, Ph.D.
City of Hope Beckman Research Institute
Duarte, CA 91010-3000
Tel: 626-218-4967
Fax: 626-471-7204
E-Mail: dann@coh.org

Abstract

Mitochondrial dynamics during nutrient starvation of cancer cells likely exert profound effects on their capability for metastatic progression. Here we report that KAP1 (TRIM28), a transcriptional co-adaptor protein implicated in metastatic progression in breast cancer, is a pivotal regulator of mitochondrial fusion in glucose-starved cancer cells. Diverse metabolic stresses induced Ser473-phosphorylation of KAP1 (pS473-KAP1) in a ROS- and p38-dependent manner. Results from live cell imaging and molecular studies revealed that during the first 6-8 hr of glucose starvation mitochondria initially underwent extensive fusion, but then subsequently fragmented in a pS473-KAP1-dependent manner. Mechanistic investigations using phosphorylation-defective mutants revealed that KAP1 Ser473-phosphorylation limited mitochondrial hyperfusion in glucose-starved breast cancer cells, as driven by downregulation of the mitofusin protein MFN2, leading to reduced oxidative phosphorylation and ROS production. In clinical specimens of breast cancer, reduced expression of MFN2 corresponded to poor prognosis in patients. In a mouse xenograft model of human breast cancer, there was an association in the core region of tumors between MFN2 downregulation and the presence of highly fragmented mitochondria. Collectively, our results suggest that KAP1 Ser473 phosphorylation acts through MFN2 reduction to restrict mitochondrial hyperfusion, thereby contributing to cancer cell survival under conditions of sustained metabolic stress.

Introduction

Cancer cells require more nutrients to support their higher proliferation compared with normal cells. For example, increased glucose uptake, also known as Warburg effect, is one of the well-characterized tumor hallmarks (1). During the course of tumor growth, cancer cells encounter various microenvironmental stresses from transient or fluctuating (acute) to diffusion-limited (chronic) hypoxia and nutrient starvation. In response to these stress conditions, cells activate a number of signaling pathways to survive diverse types of nutrient deprivation (2). One of the most prominent adaptive responses is to regulate mitochondrial dynamics (3,4). Mitochondria undergo dynamic fusion and fission processes that affect cellular biosynthetic and bioenergetic efficiency and emerging evidence suggests that dysregulated mitochondrial dynamics are associated with human diseases, including cancers (5). The balance between fragmented mitochondria and elongated mitochondria is governed by a family of GTP-dependent dynamin-related 'mitochondria-shaping' proteins (6). While the dynamic-related protein 1 (DRP1) drives mitochondrial fission, the mitofusin 1/2 (MFN1/2) and optic atrophy 1 (OPA1) proteins mediate fusion of the mitochondrial outer and inner membranes, respectively.

Based on the distance from the nearest blood vessel, tumors contain well-vascularized and poorly vascularized regions, which are thought to utilize mitochondria differently. Aerobic oxidative phosphorylation (OXPHOS) is essential for ATP production to support cell growth and is also the major intracellular source of reactive oxygen species (ROS). It has been reported that glucose deprivation induces metabolic oxidative stress via an increase in the steady-state levels of mitochondrial superoxide and hydrogen peroxide (7-10). In addition, it is also well documented that the prolonged depletion of various nutrients, such as glucose, glutamine, or arginine, induces ROS-triggered cancer cell death (11-14). Considering that mitochondrial fusion maximizes ATP generation under nutrient starvation (3,4) and that excessive ROS production is

detrimental to the cells (15), regional regulation of mitochondrial function inside the tumors becomes essential not only for bioenergetics but also for modulating intracellular redox state. Therefore, the ability of tumor cells to dynamically regulate the balance between mitochondrial fusion and fission is critical for their adaptation to metabolic stress caused by the temporal regional heterogeneity. However, the mechanisms underlying the transition from mitochondrial fusion to fission during the course of sustained nutrient depletion are not completely understood.

KRAB domain-associated protein 1 (KAP1/TRIM28) is a pleiotropic regulator of a diverse range of cellular process (16). Notably, overexpressed KAP1 has emerged as an oncogene in different types of tumors, including breast cancer (17). Previous work by us and others have shown that KAP1 is subjected to phosphorylation at multiple serine (Ser) residues, including Ser440, Ser473, Ser501 and Ser824 (16). Among these, although ATM-mediated Ser824 phosphorylation is associated with DNA damage response (18-22), the kinase responsible for and the role of KAP1 Ser473-phosphorylation (pS473-KAP1) in the context of metabolic stress is poorly understood. Here, we demonstrated that pS473-KAP1 is transiently activated following prolonged starvation by ROS-p38MAPK pathway, and pS473-KAP1 reduces mitochondrial hyperfusion, promoting colony formation in response to chronic glucose deprivation. Mechanistically, pS473-KAP1-dependent adaptive response is characterized by a reduction of MFN2. The accumulation of fragmented mitochondria in the core region, compared to the periphery, of xenografted tumors supports the regional heterogeneity of mitochondrial dynamics. Lastly, reduced MFN2 expression in breast cancer is associated with poor survival and metastasis corroborates the concept that suppression of MFN2-mediated mitochondrial fusion may underline the poor prognosis of breast cancer patients. Taken together, our studies suggest a paradigm by which ROS-p38MAPK-pS473-KAP1-MFN2 axis prevents mitochondrial

hyperfusion during the course of metabolic stress and enables breast cancer cells to survive changes in the tumor nutritional microenvironment to promote tumor growth.

Materials and Methods

Cell culture and reagents. MDA-MB-231, MDA-MB-468, MCF7, MEFs cells from ATCC, mfn2- and ampk-null MEFs cells from collaborators were obtained during the 6-years of this project from 2010 to 2015. Multiple frozen aliquots were established upon the acquisition and all experimental cells were passaged for fewer than 20-passages after reviving from liquid N_2. Cells were cultured in DMEM supplemented with 10% fetal bovine serum. MDA-MB-231/shKPA1, and MDA-MB-231/shMFN2 cells were cultured with puromycin (2 μg/ml). MDA-MB-231/shKAP1/KAP1wt, MDA-MB-231/shKAP1/KAP1S473A, MDA-MB-231/shKAP1/KAP1S473D, MDA-MB-231/shKAP1/KAP1S473A/Su9-GFP and MDA-MB-231/shKAP1/KAP1S473D/COX4-DsRed cells were maintained in the presence of puromycin (2 μg/ml) and G418 (100 μg/ml). MDA-MB-231/MFN2 cells were maintained in the presence of G418 (100 μg/ml). All nutrient depletion media were prepared with 10% dialyzed fetal bovine serum (Gibco, 26400). The glucose depletion medium was DMEM (Gibco, 11966-025) supplemented with sodium pyruvate (1 mM). The glutamine depletion medium was DMEM (Gibco, 15-013-CV). The arginine depletion medium was DMEM (Gibco, A14431-01) supplemented with L-glutamine (4 mM) and L-lysine (0.8 mM). Etomoxir (sc-215009), siRNAs against p38α (sc-29433), p38β (sc-39116) and Mfn2 (sc-43928) were from Santa Cruz biotechnology. N-acetyl-L-cysteine (A7250), Mdivi-1 (M0199), D-glucose (G7021), oligomycin A (75351), Rotenone (R8875) and FCCP (C2920) were from Sigma-Aldrich. SB203580 (152121-47-6) was from Biovision.

Plasmid and cell engineering. shRNA (TRCN0000017998) against the KAP1 3'UTR was obtained from The RNAi Consortium. MDA-MB-231/shKAP1 cells were generated using lentivirus system as described previously (12). FLAG-S473A-KAP1 and FLAG-S473D-KAP1 were engineered using FLAG-KAP1 as a template (22), respectively, by the Transformer Site Directed Mutagenesis Kit (Clonetech). The MFN2 donor vector (HsCD00039867) was obtained

from the DNASU Plasmid Repository. All KAP1 constructs were subcloned into the pDONR201 donor vector and recombined into lentiviral-gateway-compatible destination vectors with tetracycline-responsive promoter using GATEWAY technology (Invitrogen). Lentiviruses were generated as described previously (12). All constructs were validated by sequencing analyses.

Western blot analyses and antibodies. Western blot analysis was conducted as described previously(23). Antibodies used were phospho-S473-KAP1 (644602, BioLegend), phospho-S824-KAP1 (A300-767A, Bethyl), KAP1 (A300-274A, Bethyl), β-actin (MAB1501R), H3K27me^3 (07-449) from Millipore, Tom20 (sc-17764) and GAPDH (sc-25778) from Santa Cruz, phospho-T172-AMPKα (2535), AMPKα (2532), phospho-T180/Y182-p38 (9216) and p38 (9212) from Cell Signaling, MFN1 (GTX116254), MFN2 (GTX102055), OPA1 (GTX48589) and FIS1/TTC11 (GTX111010) from GeneTex, H3 (39763), H3K9me^3 (61013) from Active Motif and Mitoprofile OXPHOS Cocktail (MS601) from MitoSciences.

Cell viability, clonogenic cell survival and apoptosis assay. The acid phosphatase (ACP) assay was used to measure cell viability as described previously (12). Briefly, 5000 cells/well in the 96-well plate were seeded and incubated with different concentrations of glucose or treated with Mdivi-1 (10 μM) for 3-days. Alternatively, clonogenic cell survival was performed 48-hr after nutrient deprivation. Cells were trypsinized, combined with suspended cells, and total 100 cells were reseeded in 6-well plate for 2-weeks as described previously (7). Apoptosis was analyzed by Annexin V/Propidium iodide (PI) staining (BD Pharmingen) as described previously (12).

Soft-agar colony formation. 5,000 cells were mixed in 0.35% agarose in complete medium (top layer) and were plated on 0.7% agarose with complete medium (bottom layer) in 6-well plates. Extra medium with different concentration of glucose were added to each wells and the

medium were changed every 5-day during the 2-week of cell growth. Colonies were imaged as described previously (12).

Intracellular ROS measurement. ROS measurement was performed using DCFDA (D6883, Sigma) staining as described previously (12). Briefly, cells were stained with 1 μM DCFDA for 30-min and the resulting DCF was analyzed by flow cytometry with a maximum emission ~ 530 nm (Gallios,Beckman Coulter or BD Accuri C6). Oxidation-insensitive fluorescent DCF probe was used as a control (35848, Sigma).

RNA-seq and quantitative RT-PCR analyses. Total RNA was isolated from cells using the TRIzol reagent (15596-026, Ambion). RNA-seq was conducted by the Integrative Genomics Core at City of Hope. RNA-seq data are available in the Gene Expression Omnibus (GEO) database (GSE63344). Quantitative RT-PCR for gene expression was performed using Bio-Rad system as described previously (12). Mitochondrial D-loop primers, forward: 5'-GTGGCTTTGGAGTTGCAGTT-3'; reverse: 5'-GAAGCAGATTTGGGTACCAC-3'. *Lamin B* primers, forward: 5'-ATGAAGCGGATGTCTAAGAAAG-3'; reverse: 5'-CGCCTGGGTCCTGTTTACAC-3'.

Oxygen consumption rate. The mitochondrial OCR was measured by the Seahorse Bioscience XF24 Extracellular Flux Analyzer (Seahorse Bioscience) as described previously (12). Briefly, 6×10^4 cells were seeded in XF24 cell culture microplates overnight. On the next day, cells were washed and incubated with Mito Assay Medium (Seahorse Bioscience) supplemented with glucose (25 mM) and sodium pyruvate (1 mM). The pH value of the Mito Assay Medium was adjusted to 7.4. The OCR was assayed by sequential injections of oligomycin (1 μM), FCCP (0.5 μM) and Rotenone (2.5 μM) according to the manufacturer's instructions. After the measurements, the cells were trypsinized for cell number normalization.

ATP assay. ATP production was determined using the ENLITEN® ATP Assay System (Promega, FF2000) according to the manufacturer's instructions. Briefly, cells were harvested in cold PBS and then added to 5% trichloroacetic acid (TCA). Subsequently, tris-acetate buffer (pH 7.75) was used to neutralize the TCA solution to a final concentration of 0.1%. The extracts were further diluted 1:100 and an equal volume of rL/L Reagent (Promega, FF2000) was added to measure the luminescence using a TD-20e luminometer (Turner). The ATP amount was normalized to cell number and the relative ATP level was calculated.

Immunofluorescence staining and imaging. Tom20 antibody (sc-17764, Santa Cruz) was used for immunofluorescence staining to visualize mitochondrial morphology as described previously (12). Slides were viewed using a 60X objective on an inverted IX81 microscope (Olympus) or LSM 700 Confocal Microscope (Zeiss). Time lapse imaging was obtained by Axio Observer Z1 Inverted microscope (Zeiss) with a 20-min interval for 20-h. Videos were collected and processed using ZEN 2012 software. For Electron microscopy studies, serial block-face scanning electron microscopy (SBF-SEM) (Zeiss Sigma VP) was used. Cell pellets were prepared by the Electron Microscopy Core at City of Hope as described previously (24). Images were taken with 5400x magnification. Images were collected and processed using Image-Pro 6.3 software.

Xenograft and mouse tumor studies. Animal experiments were approved by the Institutional Animal Care and Use Committee at City of Hope. $5x10^6$ MDA-MB-231/COX4-DsRed cells were used for subcutaneous injection into the flank of 6-week-old NOD.Cg-*Prkdc*^{scid}*Il2rg*^{tm1Wjl}/SzJ (NSG) mice. KRAS-driven salivary gland tumors were generated as described previously (25). The primary tumor cells were isolated and engineered with COX4-DsRed to visualize mitochondria. $3x10^6$ cells were injected subcutaneously into the flank of

NOD.Cg-*Prkdc*^{scid}*Il2rg*^{tm1Wjl}/SzJ (NSG) mice. Mice were euthanized on day-28 to harvest tumors. Formalin-fixed, paraffin-embedded (FFPE) sections were subjected to immunohistochemistry (IHC) staining with MFN2 antibody (WH0009927M3, Sigma) by the pathology core at City of Hope. Tumors were dissected into core and peripheral regions and subjected to Western blotting analysis as described previously (26). Tumors for visualizing COX4-DsRed fluorescence were fixed in paraformaldehyde (4%) at 4°C overnight, and then subjected to 15% and 30% sucrose infiltration and O.C.T embedding. Sections were sliced at 8 μm on the cryostat (CM3050S, Leica).

Patient materials and Immunohistochemistry. The institutional review board of Chi-Mei Medical Center approved the procurement of formalin-fixed tissue and acquisition of clinical information for this study (IRB10210004). IHC staining was performed with MFN2 antibody (WH0009927M3, Sigma) as previously described (27) to assess MFN2 expression on 202 consecutively treated primary breast carcinomas underwent modified radical mastectomy without adjuvant chemotherapy between 1997 and 2002. Pathological staging was determined based on the 7th edition of American Joint Committee on Cancer (AJCC) system. Immuno-expression of MFN2 was determined by pathologists (C.F.L and T.Z.C) using H-score, defined as H-score = Σ*Pi* (*i* + 1), where *i* is the intensity of the stained tumor cells (0 to 3+), and *Pi* is the percentage of stained tumor cells for each intensity. Tumors with H-scores no less than the median of all scored cases were classified as high MFN2 expression (Table 1), as described previously (28).

Bioinformatics. The Cancer Genome Atlas (TCGA) dataset, the Netherlands Cancer Institute (NKI) dataset and Prognoscan database (http://www.prognoscan.org/) were used for data mining of mitochondrial complex genes and *KAP1* as well as the clinical relevance (29-32). Histograms were generated by software R or GraphPad Prism 6. Heatmap was generated by

GENE-E software.

Statistical Analysis. Data with error bar were presented as mean±SD. Statistical significance was determined using the two-tailed Student's *t*-test. Chi-square test was used to evaluate the correlations between MFN2 expression and various clinicopathological features. Survival analyses were performed for disease-specific and distal metastasis-free survivals. Survival curves were plotted using the Kaplan-Meier method.

Results

***KAP1* mRNA level is elevated in breast tumors and diverse nutrient stresses induce a delayed ROS-p38MAPK-dependent KAP1 phosphorylation at Ser473 in breast cancer cells.** Comparative expression analyses, based on breast cancer datasets from Netherlands Cancer Institute (NKI) (31,32), revealed that each distinct breast tumor subgroup showed a unique signature of glycolysis and OXPOS gene expression (Figure 1A). Notably, almost all breast tumors, irrespective their ER/PR/HER2 status, compared with normal-like samples, exhibited up-regulation of messages encoding proteins involved in both glycolysis and OXPHOS as well as KAP1 (Figure 1A). We further noticed that the expression of selected mitochondrial OXPHOS genes was positively associated with *KAP1* level (Supplementary Figure S1). Consistent with the study by Addison et al., showing that higher KAP1 is associated with poor prognosis in breast cancer patients (17), an elevated *KAP1* expression in breast tumors was correlated with high grades and poor prognosis (Supplementary Figure S2). We next found that glucose depletion induced a delayed (at approximately 6-h) and transient (in some cases) KAP1 phosphorylation at Ser473 (pS473-KAP1), but not Ser824 (pS824-KAP1) in triple negative breast cancer MDA-MB-231 and MDA-MB-468 cells (Figure 1B) as well as ER-positive breast cancer MCF7 cells (Figure 1C, *left panel*). Moreover, glutamine starvation (Figure 1C, *right panel*), arginine deprivation (Figure 1D, *upper panel*) and blockage of fatty acid β-oxidation by etomoxir (a CPT-1 inhibitor; Figure 1D, *lower panel*) all increased pS473-KAP1. Together, we proposed that pS473-KAP1 represents a common response to diverse nutrient starvation in breast cancer cells.

To identify the pathway for pS473-KAP1 induction, we first found that the AMPK inhibitor, compound C did not alter the glutamine starvation-induced pS473-KAP1 (Supplementary Figure S3A, *upper panel*). In parallel, pS473-KAP1 persisted in glutamine-deprived AMPKα1/AMPKα2 double knockout mouse embryonic fibroblasts (MEFs) (Supplementary Figure S3A, *lower panel*).

Similarly, we used the ATM inhibitor, Ku55933, and knockdown of CHK2 and PKCδ by small interfering (si) RNA to exclude the involvement of ATM-CHK2 (33) and PKCδ (34) pathways in inducing pS473-KAP1 under starvation (Supplementary Figures S3B, C).

Based on previous observations that metabolic stress induces ROS production in cells (7,12,13), we postulated that ROS induction activates KAP1 Ser473-phosphorylation during nutrient deprivations. Indeed, depletion of either glucose or glutamine led to a surge of oxidation of DCFDA to DCF (Supplementary Figure S3D, *left panel*), but not the oxidative-insensitive DCF analog (Supplementary Figure S3D, *right panel*), and N-acetylcysteine (NAC), a ROS scavenger, impaired starvation-induced pS473-KAP1 (Supplementary Figure S3E). Next, we found that both stress kinase p38MAPK inhibitor, SB203580, and siRNA against p38α/β attenuated starvation-induced pS473-KAP1 (Figure 1E, Supplementary Figures S3F, G). As expected, SB203580 reduced H_2O_2-induced pS473-KAP1, but not pS824-KAP1 (Supplementary Figure S3H). Lastly, previous studies have shown that NAC prevents glucose depletion-induced cell death in MCF7 cells (7). Furthermore, NAC rescued MDA-MB-231 cells from glucose depletion-induced cell death (Supplementary Figures S3I, J). Overall, our results were consistent with report by Spitz et al. that H_2O_2 produced inside cells is mediating the effects (7).

KAP1 Ser473-phosphorylation attenuates mitochondrial OXPHOS. We next explored whether pS473-KAP1 regulates ROS generation in the context of glucose deprivation. To achieve this goal, wild-type (wt)-KAP1, phosphorylation-defective S473A-KAP1 and phosphorylation-mimetic S473D-KAP1 were re-expressed in KAP1-knockdown MDA-MB-231 (MDA-MB-231/shKAP1) cells, respectively (Figure 2A, *lower panel*). Considering that mitochondrial OXPHOS is the major intracellular ROS source (35), oxygen consumption rate (OCR), reflecting the OXPHOS flux, in different KAP1-expressing cells was analyzed. As shown in Figure 2A, reconstitution of wt- and S473A-KAP1 increased both basal and FCCP-induced

maximal respiration to a higher level than S473D-KAP1 did (*upper panel*) without significant alteration on overall ATP production among these cells (Supplementary Figure S4A, *left panel*). One possibility that reduced mitochondrial number would account for the reduced OCR in S473D-KAP1-expressing cells was ruled out (Supplementary Figure S4A, *right panel*).

Given that immediate response to nutrient starvation is mitochondrial fusion to protect mitochondria from mitophagy and maximizing OXPHOS for energy generation (3,4), we explored whether pS473-KAP1 counteracts mitochondrial fusion upon nutrient deprivation. First, glucose-depletion (6-h) led to mitochondrial elongation, similar to the effect of treatment with Mdivi-1, a mitochondrial fission inhibitor (Figure 2B). Time-lapse imaging using MDA-MB-231 cells expressing mitochondria-targeted COX4-DsRed further validated this observation (Movie 1 and 2). As shown in Supplementary Figure S4B, mitochondrial fission started between 8- and 9-h post starvations, following mitochondrial fusion. Live cell imaging performed on glucose-starved, co-cultured S473A-KAP1/Su9-GFP- and S473D-KAP1/COX4-DsRed-repleted cells revealed that less elongated mitochondria were observed in the S473D-KAP1-expressing cells than in the S473A-KAP1-expressing counterparts during the course of starvation (Movies 3 and 4). Quantitative analyses based on images at 0- and 8-h post glucose starvation (Supplementary Figure S5A) validated that the expression of S473D-KAP1 alone shifted mitochondrial equilibrium towards fragmented mitochondria and that the replacement of S473A-KAP1 favored elongated mitochondria in glucose-starved MDA-MB-231/shKAP1 cells (Figure 2C). Scanning electron microscopy (SEM) analyses further confirmed that S473A-KAP1 cells harbored more elongated mitochondria with an increase in total mitochondrial surface area (Supplementary Figures S5B, C).

To assess whether unbalanced mitochondrial fusion sensitizes cells toward glucose depletion-induced cell death, we assessed cell viability of glucose-starved MDA-MB-231 cells

with (or not) Mdivi-1. Figure 2D showed that both glucose deprivation and Mdivi-1 pre-treatment increased mitochondrial maximal respiration. Moreover, Mdivi-1 pre-treatment further increased ROS signal (Figure 2E) and sensitized cells to glucose starvation-induced cell death (Supplementary Figure S5D). Likewise, expression of S473A-KAP1, but not wt- and S473D-KAP1, significantly decreased the viability of glucose-starved cells (Figure 2F). Together, these results supported a positive correlation between mitochondrial hyperfusion and elevated OCR. Notably, elevated maximal respiration could account for increased ROS generation.

pS473-KAP1 down-regulates MFN2 to limit mitochondrial fusion. To understand how pS473-KAP1 regulates mitochondrial dynamics, we compared the expression of several mitochondrial proteins during the course of glucose starvation. First, neither the steady-state levels of respective inner mitochondrial membrane complex proteins including NDUFB8 (complex I), SDHB (complex II), UQCRCII (complex III), COXII (complex IV) and ATP5A (complex V), nor the outer mitochondrial membrane protein TOM20, changed during 24-h course of glucose deprivation (Figure 3A). In contrast, a time-dependent decrease in MFN2, a mitochondrial fusion protein, was noted (Figure 3A). Likewise, arginine depletion decreased MFN2 abundance (Figure 3B). However, MFN2 abundance did not decrease in the glucose-deprived (8-h) S473A-KAP1-expressing cells (Figure 3C, *lane 7 versus lane 3*), suggesting that pS473-KAP1 down-regulates MFN2. To ascertain the role of MFN2 in regulating OXPHOS, MFN2 was knocked down in wt-, S473A- and S473D-KAP1-expressing cells. Clearly, knockdown of MFN2 markedly decreased the basal OCR in all cells and the reduced OCR in wt- and S473A-KAP1-expressing cells was comparable with the basal level of S473D-KAP1-expressing cells (Figure 3D). We also observed higher basal ROS in the S473A-KAP1 expressing cells in the presence or absence of glucose (Figure 3E). Lastly, the correlation between MFN2 and ROS level was established using wild type and *mfn2* knockout MEFs (Figure 3F). We next addressed

whether different MFN2 level affects nutrient sensitivity in MDA-MB-231 cells. As shown in Figure 3G, MFN2 over-expression and knockdown have opposite effect on nutrient sensitivity. Together with the observations on the mitochondrial hyperfusion upon arginine starvation in MDA-MB-231 cells (Supplementary Figures S5E, F), we proposed that mitochondrial hyperfusion aggravated the response to nutrient deprivation. Analyses of the RNA-seq data further uncovered additional roles for S473D-KAP1 in elevating the expression of mitochondrial complex genes (Figure 3H).

Association of MFN2 expression and mitochondrial network *in vivo*. To validate the alteration in MFN2 in response to starvation *in vivo*, xenografted MDA-MB-231/COX4-DsRed tumors were analyzed. As expected, the tumor core region, generally considered as areas undergoing metabolic stress, showed reduced MFN2 (Figures 4A - B) and with more fragmented mitochondria (Figure 4C, *upper panel*), supporting the notion that reduced MFN2 in the core region contributes to the accumulation of fragmented mitochondria via suppressed mitochondrial fusion. Next, we used a KRAS-driven mouse salivary gland tumor model developed in our laboratory recently (25) to independently validate a higher degree of mitochondrial fragmentation in the core region of tumors (Figure 4C, *lower panel*). Elevated H3K9me^3 and H3K27me^3 marks in the core region of xenografts (Figure 4B), indirectly reflecting reduced lysine demethylases (KDMs) activity due to a decrease in their cofactor, α-ketoglutarate level, attested to the regional metabolic stress inside tumors. Lastly, we sought to explore the biological consequence of metabolic stress-induced pS473-KAP1. Figure 4D revealed that S473A-KAP1-expressing cells were more sensitive to glucose reduction using an anchorage-independent cell growth assay.

To assess the pathological relevance of MFN2 level in breast cancer, we found that the loss-of-MFN2 expression was associated with adverse clinicopathological features and worse patient outcome (Table 1). Notably, MFN2 low expression was significantly associated with increments of primary tumor status (p=0.001), nodal metastasis (p=0.033), and stage (p=0.002) (Figure 5A). Multivariate analysis showed that loss-of-MFN2 expression, along with higher stage, remained to be prognostically significant for disease-specific (p=0.0024) and metastasis-free (p<0.0001) survival (Figure 5B). Consistently, the TCGA breast cancer dataset showed that *MFN2* message was lower in breast tumors compared to normal tissues (Figures 5C). Data mining on PrognoScan database (http://www.prognoscan.org/) (29) showed that reduced *MFN2* message was correlated with poor survivals (Figures 5D - G). Altogether, our results highlighted the importance of p38/pS473-KAP1/MFN2 pathway in promoting tumor cells' survival under metabolic stress.

Discussion

Cancer cells are usually in a state of chronic oxidative stress and use higher glucose and hydroperoxide metabolism for compensation. Therefore, targeting glycolysis and antioxidant pathways could be therapeutic strategies for cancer (9,36,37). On the other hand, mitochondrial O_2 metabolism is critical for the further induction of oxidative stress in cancer upon nutrient starvation such as glucose depletion (8,37). Our current findings extend the repertoire of critical cellular processes initiated by nutrient starvation, including the induction of pS473-KAP1 through ROS-/p38MAPK-dependent pathway and the subsequent down-regulation of MFN2, to reduce mitochondrial hyperfusion and OXPHOS in order to ameliorate metabolic oxidative stress. Although our pharmacological and genetic approaches suggested the involvement of p38 in this process, the specific role of different p38 isoforms in the context of distinct metabolic stress remained obscure, and as such, whether other kinases also mediate oxidative stress-induced pS473-KAP1 signaling needs further study in the future. Presumably, metabolic stress-triggered pS473-KAP1 is a general phenomenon present in both normal and tumor cells. However, since proliferating tumor cells usually exhibit higher oxidative stress and metabolic demands, this signaling pathway could be more prominent in cancer and depend on cells' nutrient dependency. For example, the fact that MCF7 cells are more glutamine-independent (38) could partially explain why glutamine deprivation-induced pS473-KAP1 was less robust in MCF7 cells (Figure 1C). It is likely that primary mammary epithelial cells are relatively resistant to glucose depletion (36). As shown in Figure 6, we propose that pS473-KAP1-mediated MFN2 down-regulation is crucial for overcoming nutrient stress during tumor growth.

Upon prolonged metabolic stress, we noted a marked down-regulation of MFN2 that limits the initial hyperfusion response. Although MFN1, another mitofusin, is present, it apparently is unable to compensate for the loss of MFN2. This behavior is consistent with previous

observations that disruption of either *mitofusin* gene leads to severe mitochondrial fragmentation (39). Clinically, we found lower MFN2 expression correlated with more malignant breast tumors, which is consistent with earlier reports proposing MFN2 as a tumor suppressor (40-42). The mechanisms underlying the control of mitochondrial dynamics in cancer cells received more attention recently. For example, Drp1-mediated mitochondrial fission is linked to tumor transformation (43,44). Moreover, more mitochondrial fission is observed in lung cancer compared with normal lung cells, and inhibition of mitochondrial fission induces cancer cell death (45). Fragmented mitochondria have been shown to promote breast cancer metastasis (46). These observations and our results together put mitochondrial dynamics control squarely in the driver's seat of tumor progression and support the notion that MFN2 down-regulation represents an additional layer mechanism of preventing mitochondrial hyperfusion process during tumorigenesis.

It has been reported that OCR was elevated under low glucose (0.75 mM) (47) and that shifting carbon source from glucose to galactose or acetoacetate induced OCR and subsequent mitochondrial elongation (48), attesting to our observations that short-term (< 6-h) starvation of glucose increased OCR. Although up-regulation of mitochondrial OXPHOS is beneficial as a short-term response to acute nutrient starvation, the increased ROS production from elongated mitochondria would in turn cause cell death during prolonged starvation. Collectively, our data provide a new mechanistic insight into how activation of the KAP1-/MFN2-dependent arm copes with metabolic oxidative stress. Given that most cancer cells displayed elevated ROS (49), drugs targeting this regulatory circuit could have a positive therapeutic impact by sensitizing cancer cells to oxidative stress-based therapeutic strategies.

To our knowledge, this is the first study demonstrating that KAP1 can be post-translationally modified upon metabolic stress. Ideally, we would like to observe a gradient of pS473-KAP1

signals, opposite to the MFN2 levels in solid tumors. However, due to the lack of the availability of IHC-quality pS473-KAP1 antibody, our repeated efforts failed to detect any pS473-KAP1 signal using FFPE specimens of either primary patient samples or xenografted tumors. Moreover, whether other post-translational modifications of KAP1 also occur under nutrient deprivation to regulate metabolic stress response deserves more attention. In the current study, we demonstrated that pS473-KAP1 is associated with MFN2 down-regulation upon metabolic stress. Although the detailed molecular mechanism is unclear, it is possible that KAP1 directly or indirectly regulates MFN2 abundance. Based on our unpublished observations, several microRNAs are up-regulated in S473D-KAP1-re-expressing cells. Among these, potential starvation-induced and MFN2-targeting microRNA is identified and under investigation.

In conclusion, we show that ROS-/p38MAPK-induced pS473-KAP1, following the initial induction of mitochondrial fusion, prevents mitochondrial hyperfusion by down-regulating MFN2, thus promoting the survival of metabolically stressed tumor cells. Our findings not only identify a marker(s) potentially useful for breast cancer stratification but also a mechanistic link for tumor cells to adapt to metabolic stresses during tumor progression and cancer therapy.

Acknowledgements

We are sincerely grateful to Drs. Emily Wang and Art Riggs for their helpful suggestions and critical reading of manuscript, Ms. Lucy Brown of the Analytical Cytometry Core for flow cytometry analyses, Dr. Brian Armstrong and Ms. Tina Patel of the Light Microscopy Core for microscopy analyses, Mr. Austin Changou for processing time lapse imaging analyses, Drs. Xiwei Wu and Jinhui Wang and Mr. Charles Warden of Functional Genomics Core for RNA-seq data analyses, Ms. Tina Montgomery and Ms. Sofia Loera of Pathology Core for immunohistochemical analyses, Dr. Tzu-Ju Chen for pathological evaluation, Drs. Marcia Miller, Zhuo Li and Ricardo Zerda of Electron Microscopy Core and Mr. Kevin Chi for EM image analysis and members of Dr. Ann's laboratory for helpful discussions and Dr. Nancy Linford for editing.

References

1. Vander Heiden MG, Cantley LC, Thompson CB. Understanding the Warburg Effect: The Metabolic Requirements of Cell Proliferation. Science 2009;324(5930):1029-33.
2. Cairns RA, Harris IS, Mak TW. Regulation of cancer cell metabolism. Nat Rev Cancer 2011;11(2):85-95.
3. Gomes LC, Benedetto GD, Scorrano L. During autophagy mitochondria elongate, are spared from degradation and sustain cell viability. Nat Cell Biol 2011;13(5):589-98.
4. Rambold AS, Kostelecky B, Elia N, Lippincott-Schwartz J. Tubular network formation protects mitochondria from autophagosomal degradation during nutrient starvation. Proc Natl Acad Sci U S A 2011;108(25):10190-95.
5. Grandemange S, Herzig S, Martinou J-C. Mitochondrial dynamics and cancer. Semin Cancer Biol 2009;19(1):50-56.
6. Lackner L. Shaping the dynamic mitochondrial network. BMC Biol 2014;12(1):35.
7. Lee YJ, Galoforo SS, Berns CM, Chen JC, Davis BH, Sim JE, et al. Glucose Deprivation-induced Cytotoxicity and Alterations in Mitogen-activated Protein Kinase Activation Are Mediated by Oxidative Stress in Multidrug-resistant Human Breast Carcinoma Cells. J Biol Chem 1998;273(9):5294-99.
8. Spitz DR, Sim JE, Ridnour LA, Galoforo SS, Lee YJ. Glucose Deprivation-Induced Oxidative Stress in Human Tumor Cells: A Fundamental Defect in Metabolism? Ann N Y Acad Sci 2000;899(1):349-62.
9. Ahmad IM, Aykin-Burns N, Sim JE, Walsh SA, Higashikubo R, Buettner GR, et al. Mitochondrial and H2O2 Mediate Glucose Deprivation-induced Stress in Human Cancer Cells. J Biol Chem 2005;280(6):4254-63.
10. Aykin-Burns N, Ahmad Iman M, Zhu Y, Oberley Larry W, Spitz Douglas R. Increased levels of superoxide and H2O2 mediate the differential susceptibility of cancer cells versus normal cells to glucose deprivation. Biochem J 2009;418(1):29-37.
11. Hensley CT, Wasti AT, DeBerardinis RJ. Glutamine and cancer: cell biology, physiology, and clinical opportunities. J Clin Invest 2013;123(9):3678-84.
12. Qiu F, Chen Y-R, Liu X, Chu C-Y, Shen L-J, Xu J, et al. Arginine Starvation Impairs Mitochondrial Respiratory Function in ASS1-Deficient Breast Cancer Cells. Sci Signal 2014;7(319):ra31.
13. Changou CA, Chen Y-R, Xing L, Yen Y, Chuang FYS, Cheng RH, et al. Arginine starvation-associated atypical cellular death involves mitochondrial dysfunction, nuclear DNA leakage, and chromatin autophagy. Proc Natl Acad Sci U S A 2014;111(39):14147-52.

14. Graham NA, Tahmasian M, Kohli B, Komisopoulou E, Zhu M, Vivanco I, et al. Glucose deprivation activates a metabolic and signaling amplification loop leading to cell death. Mol Syst Biol 2012;8:589.
15. Fruehauf JP, Meyskens FL. Reactive Oxygen Species: A Breath of Life or Death? Clin Cancer Res 2007;13(3):789-94.
16. Cheng C-T, Kuo C-Y, Ann DK. KAPtain in charge of multiple missions: Emerging roles of KAP1. World J Biol Chem 2014;5(3):308-20.
17. Addison J, Koontz C, Fugett JH, Creighton CJ, Chen D, Farrugia MK, et al. KAP1 promotes proliferation and metastatic progression of breast cancer cells. Cancer Res 2014;75(2):344-55.
18. White DE, Negorev D, Peng H, Ivanov AV, Maul GG, Rauscher FJ. KAP1, a Novel Substrate for PIKK Family Members, Colocalizes with Numerous Damage Response Factors at DNA Lesions. Cancer Res 2006;66(24):11594-99.
19. Ziv Y, Bielopolski D, Galanty Y, Lukas C, Taya Y, Schultz DC, et al. Chromatin relaxation in response to DNA double-strand breaks is modulated by a novel ATM- and KAP-1 dependent pathway. Nat Cell Biol 2006;8(8):870-76.
20. Nozomi T, Bipasha M, Sandeep B. Distinct roles of ATR and DNA-PKcs in triggering DNA damage responses in ATM-deficient cells. EMBO Rep 2009;10(6):629-35.
21. Li X, Lee Y-K, Jeng J-C, Yen Y, Schultz DC, Shih H-M, et al. Role for KAP1 Serine 824 Phosphorylation and Sumoylation/Desumoylation Switch in Regulating KAP1-mediated Transcriptional Repression. J Biol Chem 2007;282(50):36177-89.
22. Lee Y-K, Thomas SN, Yang AJ, Ann DK. Doxorubicin Down-regulates Krüppel-associated Box Domain-associated Protein 1 Sumoylation That Relieves Its Transcription Repression on p21WAF1/CIP1 in Breast Cancer MCF-7 Cells. J Biol Chem 2007;282(3):1595-606.
23. Kuo C-Y, Li X, Kong X-Q, Luo C, Chang C-C, Chung Y, et al. An Arginine-rich Motif of Ring Finger Protein 4 (RNF4) Oversees the Recruitment and Degradation of the Phosphorylated and SUMOylated Krüppel-associated Box Domain-associated Protein 1 (KAP1)/TRIM28 Protein during Genotoxic Stress. J Biol Chem 2014;289(30):20757-72.
24. West JB, Fu Z, Deerinck TJ, Mackey MR, Obayashi JT, Ellisman MH. Structure–function studies of blood and air capillaries in chicken lung using 3D electron microscopy. Respir Physiol Neurobiol 2010;170(2):202-09.
25. Fu Y, Cruz-Monserrate Z, Helen Lin H, Chung Y, Ji B, Lin S-m, et al. Ductal activation of oncogenic KRAS alone induces sarcomatoid phenotype. Sci Rep 2015;5:13347.
26. Lin HH, Lin SM, Chung Y, Vonderfecht S, Camden JM, Flodby P, et al. Dynamic involvement of ATG5 in cellular stress responses. Cell Death Dis 2014;5:e1478.

27. Li C-F, Chen L-T, Lan J, Chou F-F, Lin C-Y, Chen Y-Y, et al. AMACR amplification and overexpression in primary imatinib-naïve gastrointestinal stromal tumors: a driver of cell proliferation indicating adverse prognosis. Oncotarget 2014.
28. Lee S-W, Li C-F, Jin G, Cai Z, Han F, Chan C-H, et al. Skp2-Dependent Ubiquitination and Activation of LKB1 Is Essential for Cancer Cell Survival under Energy Stress. Mol Cell 2015;57(6):1022-33.
29. Mizuno H, Kitada K, Nakai K, Sarai A. PrognoScan: a new database for meta-analysis of the prognostic value of genes. BMC Med Genomics 2009;2(1):18.
30. Marx V. Drilling into big cancer-genome data. Nat Meth 2013;10(4):293-97.
31. van Vliet M, Reyal F, Horlings H, van de Vijver M, Reinders M, Wessels L. Pooling breast cancer datasets has a synergetic effect on classification performance and improves signature stability. BMC Genomics 2008;9(1):375.
32. van de Vijver MJ, He YD, van 't Veer LJ, Dai H, Hart AAM, Voskuil DW, et al. A Gene-Expression Signature as a Predictor of Survival in Breast Cancer. N Engl J Med 2002;347(25):1999-2009.
33. Hu C, Zhang S, Gao X, Gao X, Xu X, Lv Y, et al. Roles of the KRAB-associated co-repressor KAP1 S473 phosphorylation in DNA damage response. J Biol Chem 2012;287(23):18937-52.
34. Chang C-W, Chou H-Y, Lin Y-S, Huang K-H, Chang C-J, Hsu T-C, et al. Phosphorylation at Ser473 regulates heterochromatin protein 1 binding and corepressor function of TIF1beta/KAP1. BMC Mol Biol 2008;9(1):61.
35. Murphy MP. How mitochondria produce reactive oxygen species. Biochem J 2009;417(1):1-13.
36. Fath MA, Ahmad IM, Smith CJ, Spence J, Spitz DR. Enhancement of Carboplatin-Mediated Lung Cancer Cell Killing by Simultaneous Disruption of Glutathione and Thioredoxin Metabolism. Clin Cancer Res 2011;17(19):6206-17.
37. Hadzic T, Aykin-Burns N, Zhu Y, Coleman MC, Leick K, Jacobson GM, et al. Paclitaxel combined with inhibitors of glucose and hydroperoxide metabolism enhances breast cancer cell killing via H2O2-mediated oxidative stress. Free Radic Biol Med 2010;48(8):1024-33.
38. Kung H-N, Marks JR, Chi J-T. Glutamine Synthetase Is a Genetic Determinant of Cell Type–Specific Glutamine Independence in Breast Epithelia. PLoS Genet 2011;7(8):e1002229.
39. Chen H, Detmer SA, Ewald AJ, Griffin EE, Fraser SE, Chan DC. Mitofusins Mfn1 and Mfn2 coordinately regulate mitochondrial fusion and are essential for embryonic development. J Cell Biol 2003;160(2):189-200.

40. Wu L, Li Z, Zhang Y, Zhang P, Zhu X, Huang J, et al. Adenovirus-expressed human hyperplasia suppressor gene induces apoptosis in cancer cells. Mol Cancer Ther 2008;7(1):222-32.
41. Chen K-H, Dasgupta A, Ding J, Indig FE, Ghosh P, Longo DL. Role of mitofusin 2 (Mfn2) in controlling cellular proliferation. FASEB J 2014;28(1):382-94.
42. Zhang G-E, Jin H-L, Lin X-K, Chen C, Liu X-S, Zhang Q, et al. Anti-Tumor Effects of Mfn2 in Gastric Cancer. Int J Mol Sci 2013;14(7):13005-21.
43. Serasinghe Madhavika N, Wieder Shira Y, Renault Thibaud T, Elkholi R, Asciolla James J, Yao Jonathon L, et al. Mitochondrial Division Is Requisite to RAS-Induced Transformation and Targeted by Oncogenic MAPK Pathway Inhibitors. Mol Cell;57(3):521-36.
44. Kashatus Jennifer A, Nascimento A, Myers Lindsey J, Sher A, Byrne Frances L, Hoehn Kyle L, et al. Erk2 Phosphorylation of Drp1 Promotes Mitochondrial Fission and MAPK-Driven Tumor Growth. Mol Cell;57(3):537-51.
45. Rehman J, Zhang HJ, Toth PT, Zhang Y, Marsboom G, Hong Z, et al. Inhibition of mitochondrial fission prevents cell cycle progression in lung cancer. FASEB J 2012;26(5):2175-86.
46. Zhao J, Zhang J, Yu M, Xie Y, Huang Y, Wolff DW, et al. Mitochondrial dynamics regulates migration and invasion of breast cancer cells. Oncogene 2013;32(40):4814-24.
47. Birsoy K, Possemato R, Lorbeer FK, Bayraktar EC, Thiru P, Yucel B, et al. Metabolic determinants of cancer cell sensitivity to glucose limitation and biguanides. Nature 2014;508(7494):108-12.
48. Mishra P, Carelli V, Manfredi G, Chan David C. Proteolytic Cleavage of Opa1 Stimulates Mitochondrial Inner Membrane Fusion and Couples Fusion to Oxidative Phosphorylation. Cell Metab 2014;19(4):630-41.
49. Trachootham D, Alexandre J, Huang P. Targeting cancer cells by ROS-mediated mechanisms: a radical therapeutic approach? Nat Rev Drug Discov 2009;8(7):579-91.

Table 1. Correlation between MFN2 expression and various clinicopathological factors.

Parameters	Category	No. of case	MFN2 Expression		*p*-valuve
			High Exp.	Low Exp.	
Age (years)	<60 years	141	73	68	0.444
	≧60 years	61	28	33	
Primary tumor (T)	T1	82	53	29	**0.001***
	T2	96	35	61	
	T3-4	24	13	11	
Nodal status (N)	N0	117	66	51	**0.033***
	N1-N2	85	35	50	
Stage	I	63	43	20	**0.002***
	II	115	48	67	
	III	24	10	14	
Histological grade	Grade I	18	13	5	**0.022***
	Grade II	141	73	68	
	Grade III	43	15	28	

***: Statistically significant**

Figure legends

Figure 1. Diverse metabolic stresses induce KAP1 Ser473-phosphorylation in breast cancer cells. (A) *Overexpression of metabolic genes and KAP1 in breast cancers.* Genes were selected from 103 NKI samples based on Kyoto Encyclopedia of Genes and Genomes (KEGG) database to generate heatmap. **(B)** *Glucose depletion induces dose- and time-dependent KAP1 Ser473-phosphorylation in TNBC cells*. MDA-MB-231 cells were incubated with the indicated concentrations of glucose for 24-h (*upper panel*). MDA-MB-231 and MDA-MB-468 cells were cultured in glucose-depleted medium for different time periods as indicated (*2nd and 3rd panels*). Non-contiguous lanes were separated by a dashed line. **(C, D)** *Induction of pS473-KAP1 by diverse metabolic stresses in MDA-MB-231 and MCF7 cells.* **(C)** MDA-MB-231 (*right panel*) and MCF7 (*left panel*) cells were starved of glucose or glutamine or treated with 2-DG as indicated. **(D)** *Arginine depletion or Etomoxir induces time-dependent KAP1 Ser473-phosphorylation in MDA-MB-231 cells*. MDA-MB-231 cells were subjected to arginine depletion (*upper panel*). MDA-MB-231 and MCF7 cells were treated with increasing concentrations of Etomoxir (*lower panel*). **(E)** *Blocking p38 signaling blunts glucose and glutamine depletion-induced pS473-KAP1.* SB203580 reduced glucose or glutamine depletion-induced pS473-KAP1 (*upper panel*). p38α knockdown dampened pS473-KAP1 induction in response to glucose depletion (*lower panel*). p-p38: T180/Y182-phosphorylated p38MAPK.

Figure 2. KAP1 Ser473 phosphorylation reduces the level of glucose deprivation-promoted mitochondrial fusion. (A) *Knockdown of KAP1 or repletion with S473D-KAP1 reduces basal and maximal mitochondrial respiration.* OCR was measured (*upper panel*) in different KAP1-expressing cells (*lower panel*). Mean±SD from n=3. **(B)** *Glucose depletion promotes mitochondrial fusion*. MDA-MB-231 cells were pre-treated with vehicle or Mdivi-1 (20

μM) for 18-h prior to glucose starvation. Arrowhead: tubulated mitochondria; scale bar: 10 μm; n>3. **(C)** *Expression of S473A-KAP1 favors mitochondrial fusion in glucose-starved MDA-MB-231/shKAP1 cells.* Representative images of the typical fragmented, intermediate and tubulated mitochondrial network are shown (*left panel*). Quantitation (%) of cells with each mitochondrial morphology (*right panel*; n=80; also see Supplementary Figure S5A). **(D)** *Mdivi-1 treatment mirrors glucose starvation to induce basal and maximal mitochondrial respiration*. MDA-MB-231 cells were pre-treated with vehicle or Mdivi-1 (20 μM) for 18-h prior to glucose starvation (6-h); n=3. **(E)** *Mdivi-1 further induces the ROS level after glucose depletion.* MDA-MB-231 cells were treated as in (**D**); n=3. **(F)** *Repletion of S473A-KAP1 sensitizes MDA-MB-231/shKAP1 cells to glucose depletion*. Cells were incubated with the decreasing concentrations of glucose for 72-h. Mean±SD from n=3; *: $p<0.05$, ***: $p<0.001$.

Figure 3. KAP1 Ser473 phosphorylation reduces OCR via MFN2 down-regulation and regulates mitochondrial gene expression. (A) *Glucose depletion down-regulates MFN2 protein abundance*. **(B)** *Arginine depletion down-regulates MFN2 in MDA-MB-231 cells.* **(C)** *KAP1 S473A substitution retards MFN2 down-regulation in glucose-starved MDA-MB-231/shKAP1 cells.* Relative MFN2 abundance is calculated by designating the level in control MDA-MB-231 cells **(A, B)** or MDA-MB-231/shKAP1 cells **(C)** as 1 after normalization with GAPDH and shown in *italic*. **(D)** *Knockdown of MFN2 reduces basal OCR in different KAP1-expressing cells*. MFN2 was knocked down by siRNA in different KAP1-expressing cells. SA: S473A-KAP1, SD: S473D-KAP1. **(E)** *The ROS level is higher in S473A-KAP1 re-expressing MDA-MB-231/shKAP1 cells*. Cells were cultured in complete (Ctrl) or glucose depletion medium (Glc-) for 6-h. Relative oxidized DCF levels were calculated by designating the value in wt-KAP1 re-expressing MDA-MB-231/shKAP1 as 1. **(F)** *ROS level is reduced in mfn2-/- MEFs*. Relative oxidized DCF levels were calculated by designating the value in wt MEFs as 1. **(G)** *Knockdown*

and overexpression of MFN2 have opposite effect on cell viability under different nutrient starvation. Clonogenic survival fraction was calculated by designating cells in complete medium as 1. **(D - G)** Mean±SD from n=3; *: $p<0.05$, **: $p<0.01$, ***: $p<0.01$. **(H)** *S473D-KAP1 elevates expression of the mitochondrial complex genes.* Relative message abundance was calculated by designating the respective message abundance in wt-KAP1-expressing MDA-MB-231/shKAP1 cells as 1.

Figure 4. MFN2 down-regulation is associated with mitochondrial fission in the core region of tumor. (A) *A gradient decrease of MFN2 staining inwards to the core region of MDA-MB-231/COX4-DsRed xenografts by IHC.* Dotted lines depict borders of different regions as shown in the diagram (*inset*). Scale bar: 100 μm; n=2. **(B)** *MFN2* is down-regulated in the core region of xenografted tumors. P: Peripheral region; C: Core; n=2. **(C)** *Mitochondria are more fragmented in the core region of tumors*. Mitochondrial morphologies are visualized with COX4-DsRed in xenografted MDA-MB-231 cells (*upper panel*) and K-RAS^{G12V}-driven mouse salivary duct carcinoma (*lower panel*). Insets: enlarged views *(upper panel)*; scale bar: 100 μm (*upper panel*) and 10 μm (*lower panel*). **(D)** *Repletion of S473A-KAP1 reduces colony formation in MDA-MB-231/shKAP1 cells*. n=3 *: $p<0.05$; ***: $p<0.005$.

Figure 5. Association of MFN2 with clinical prognosis. (A - G) *Lower MFN2 is associated with adverse clinical features.* **(A)** *Reduced MFN2 expression is correlated with malignant breast tumors*. Inversed MFN2 expression in low (*panel a*) and high (*panel b*) stage breast carcinoma and paired primary breast carcinoma (*panel c*) and its nodal deposition (*panel d*). **(B)** *Reduced MFN2 expression is correlated with poor disease-specific and metastasis-free survival*. **(A, B)** 202 primary breast cancer samples from Chi-Mei Medical Center were used (also see Table 1). **(C)** *MFN2 transcript level is down-regulated in primary and metastatic breast tumors compared*

with normal tissues. The TCGA dataset was used. **: $p<0.01$; ***: $p<0.005$. **(D - G)** *PrognoScan database-based Kaplan-Meier analysis in breast cancer datasets.* The data are retrieved from the Gene Expression Omnibus (http://www.ncbi.nlm.nih.gov/geo) with the accession numbers GSE9893 **(D)**, GSE11121 **(E)**, GSE1379 **(F)** and GSE2990 **(G)**, respectively.

Figure 6. A KAP1/MFN2-dependent arm prevents mitochondrial hyperfusion during the course of metabolic stress. To maximize the utilization of available nutrients, mitochondria undergo fusion, which would generate excessive ROS in tumor cells distant from blood vessel. The elevated oxidative stress subsequently results in p38MAPK mediated pS473-KAP1 induction. pS473-KAP1 then suppresses mitochondrial hyperfusion via MFN2 down-regulation.

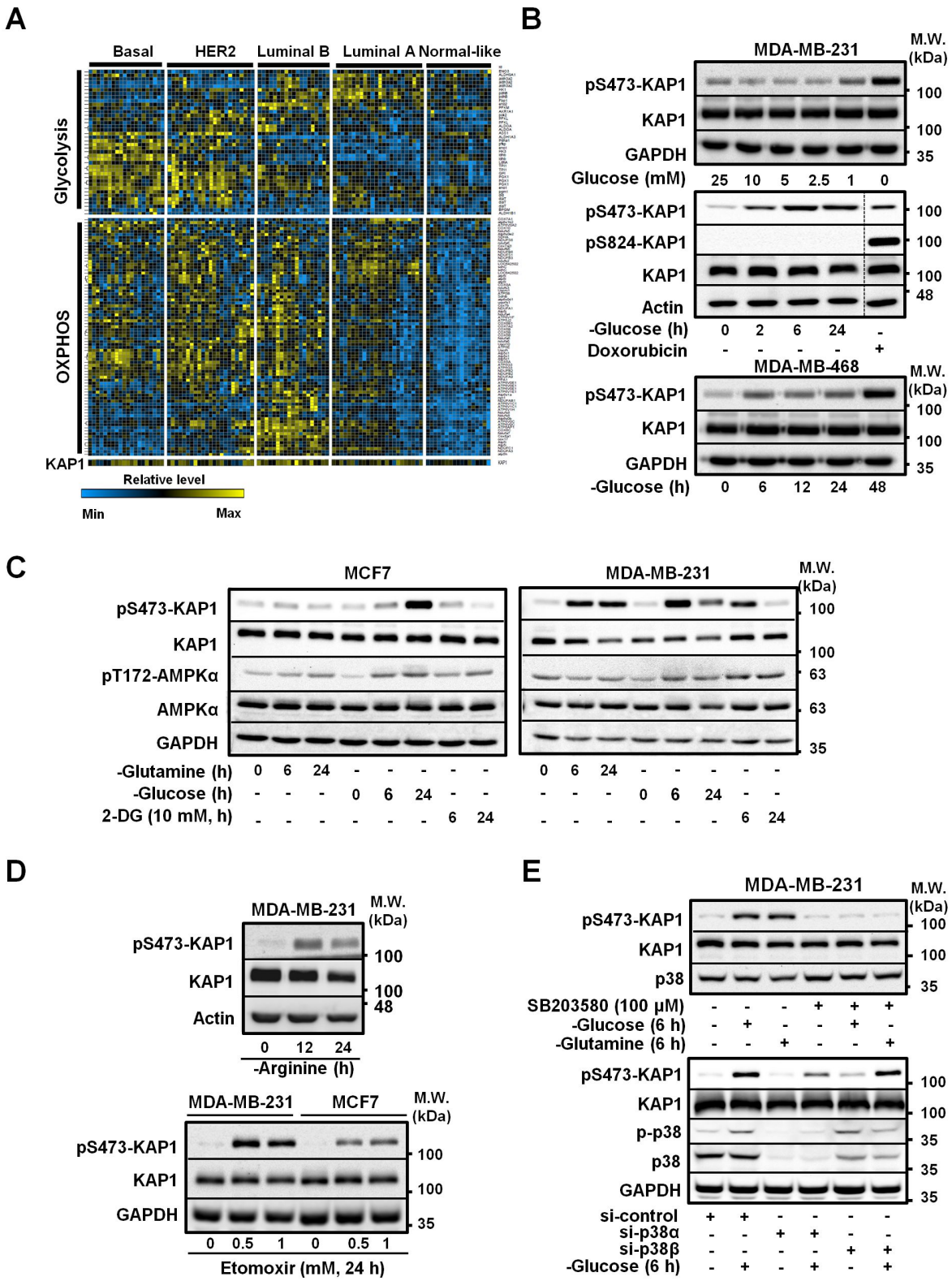
A
Basal
HER2
Luminal B
Luminal A
Normal-like
Glycolysis
OXPHOS
KAP1
Relative level
Min
Max
B
MDA-MB-231
M.W. (kDa)
pS473-KAP1
KAP1
GAPDH
Glucose (mM)
25 10 5 2.5 1 0
pS473-KAP1
pS824-KAP1
KAP1
Actin
-Glucose (h)
0 2 6 24 -
Doxorubicin
- - - - +
MDA-MB-468
pS473-KAP1
KAP1
GAPDH
-Glucose (h)
0 6 12 24 48
C
MCF7
MDA-MB-231
M.W. (kDa)
pS473-KAP1
KAP1
pT172-AMPKα
AMPKα
GAPDH
-Glutamine (h)
0 6 24 - - - - -
-Glucose (h)
- - - 0 6 24 - -
2-DG (10 mM, h)
- - - - - - 6 24
D
MDA-MB-231
M.W. (kDa)
pS473-KAP1
KAP1
Actin
0 12 24
-Arginine (h)
MDA-MB-231
MCF7
M.W. (kDa)
pS473-KAP1
KAP1
GAPDH
0 0.5 1 0 0.5 1
Etomoxir (mM, 24 h)
E
MDA-MB-231
M.W. (kDa)
pS473-KAP1
KAP1
p38
SB203580 (100 μM)
-Glucose (6 h)
-Glutamine (6 h)
pS473-KAP1
KAP1
p-p38
p38
GAPDH
si-control
si-p38α
si-p38β
-Glucose (6 h)

Fig. 1

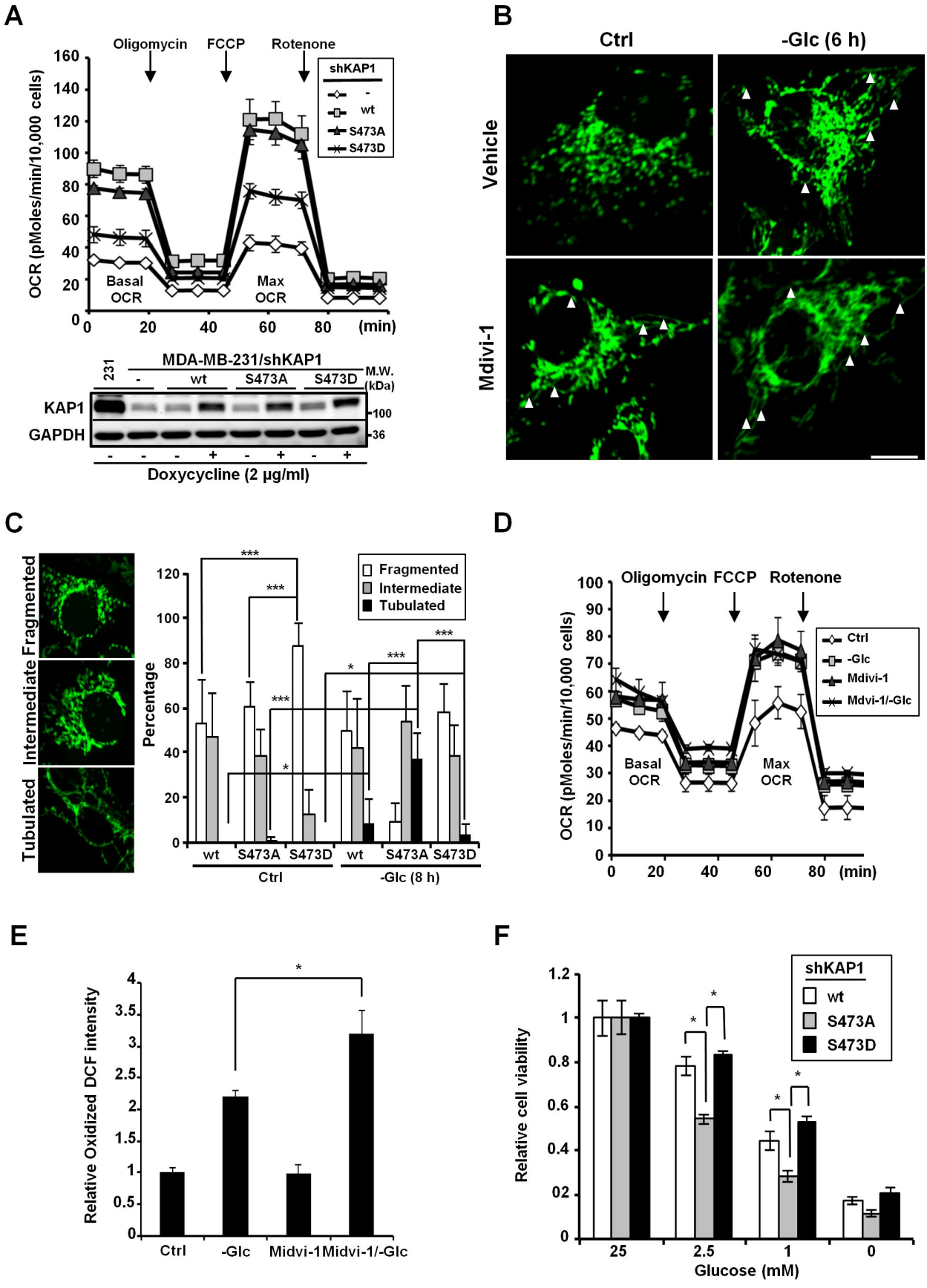
A
Oligomycin
FCCP
Rotenone
shKAP1
-
wt
S473A
S473D
OCR (pMoles/min/10,000 cells)
Basal OCR
Max OCR
(min)
MDA-MB-231/shKAP1
231
M.W. (kDa)
KAP1
GAPDH
100
36
Doxycycline (2 μg/ml)
B
Ctrl
-Glc (6 h)
Vehicle
Mdivi-1
C
Fragmented
Intermediate
Tubulated
Percentage
Ctrl
-Glc (8 h)
D
Oligomycin
FCCP
Rotenone
Ctrl
-Glc
Mdvi-1
Mdvi-1/-Glc
OCR (pMoles/min/10,000 cells)
Basal OCR
Max OCR
(min)
E
Relative Oxidized DCF intensity
Ctrl
-Glc
Midvi-1
Midvi-1/-Glc
F
shKAP1
wt
S473A
S473D
Relative cell viability
Glucose (mM)

Fig. 2

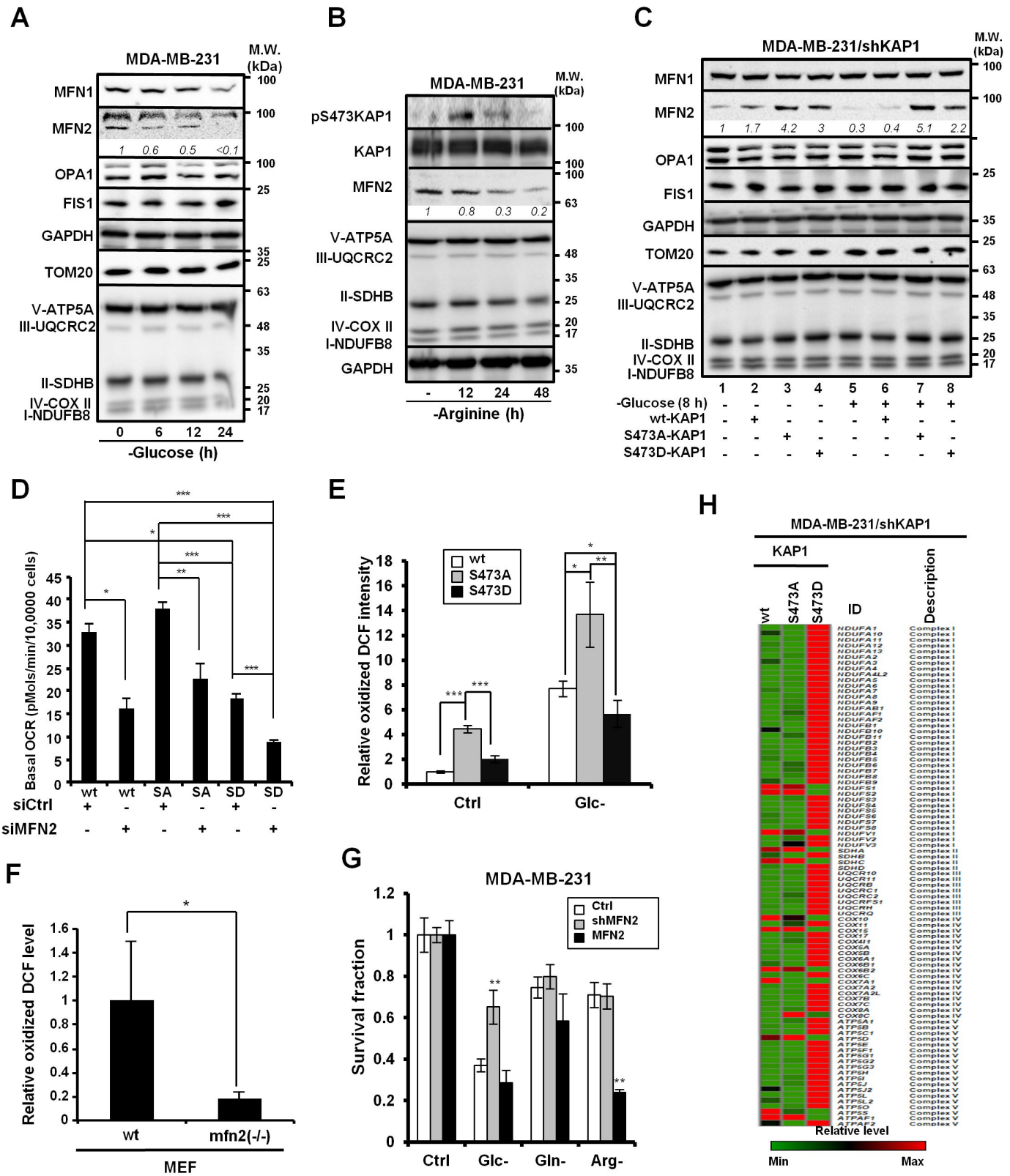
A
MDA-MB-231
M.W. (kDa)
MFN1
MFN2
1 0.6 0.5 <0.1
OPA1
FIS1
GAPDH
TOM20
V-ATP5A
III-UQCRC2
II-SDHB
IV-COX II
I-NDUFB8
0 6 12 24
-Glucose (h)
B
MDA-MB-231
pS473KAP1
KAP1
MFN2
1 0.8 0.3 0.2
V-ATP5A
III-UQCRC2
II-SDHB
IV-COX II
I-NDUFB8
GAPDH
- 12 24 48
-Arginine (h)
C
MDA-MB-231/shKAP1
MFN1
MFN2
1 1.7 4.2 3 0.3 0.4 5.1 2.2
OPA1
FIS1
GAPDH
TOM20
V-ATP5A
III-UQCRC2
II-SDHB
IV-COX II
I-NDUFB8
-Glucose (8 h)
wt-KAP1
S473A-KAP1
S473D-KAP1
D
Basal OCR (pMols/min/10,0000 cells)
wt wt SA SA SD SD
siCtrl
siMFN2
E
Relative oxidized DCF intensity
wt
S473A
S473D
Ctrl
Glc-
F
Relative oxidized DCF level
wt
mfn2(-/-)
MEF
G
MDA-MB-231
Survival fraction
Ctrl
shMFN2
MFN2
Ctrl Glc- Gln- Arg-
H
MDA-MB-231/shKAP1
KAP1
wt S473A S473D
ID
Description
Relative level
Min
Max

Fig. 3

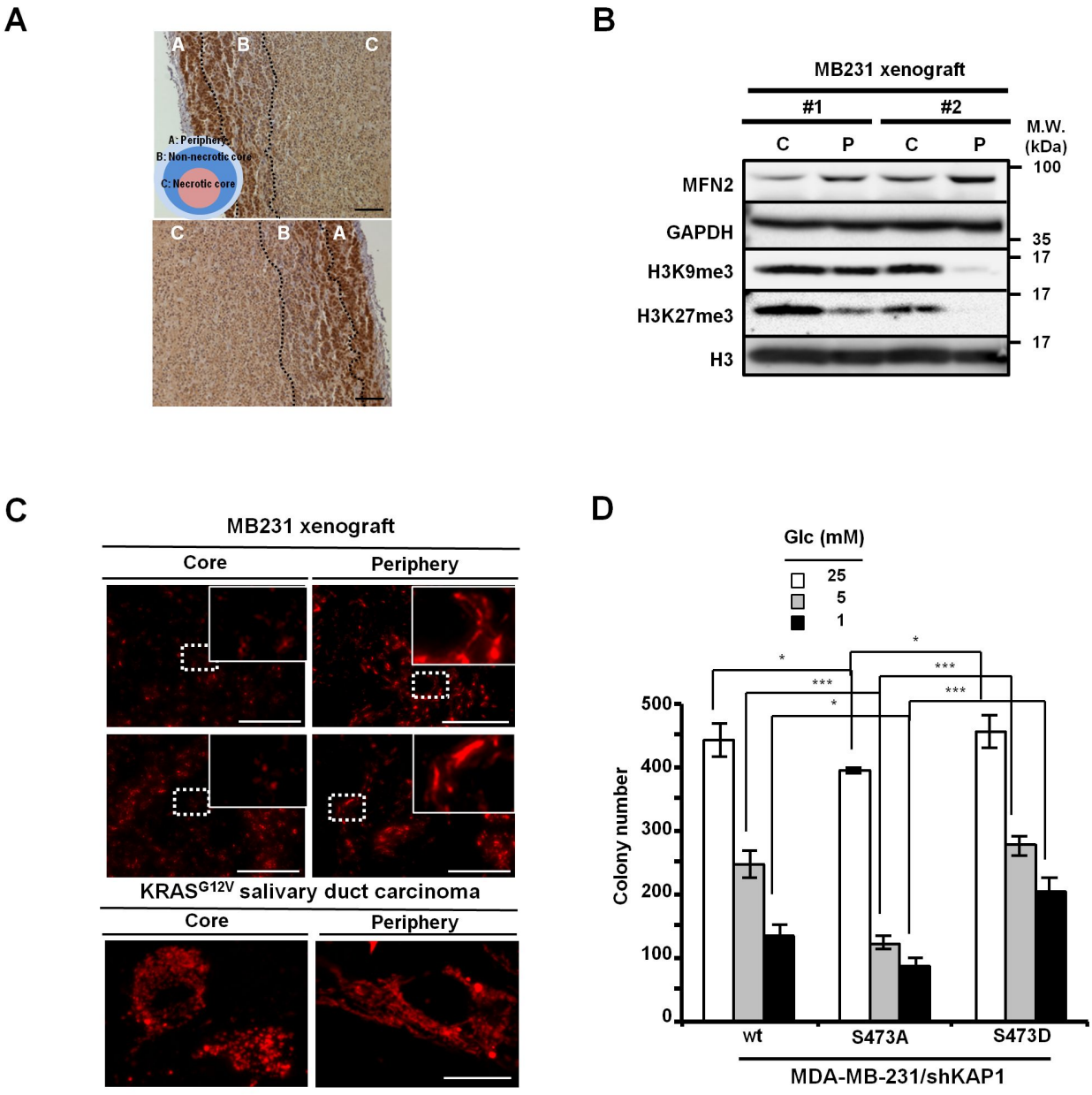
A
A
B
C
A: Periphery
B: Non-necrotic core
C: Necrotic core
C
B
A
B
MB231 xenograft
#1
#2
C
P
C
P
M.W. (kDa)
MFN2
GAPDH
H3K9me3
H3K27me3
H3
100
35
17
17
17
C
MB231 xenograft
Core
Periphery
KRASG12V salivary duct carcinoma
Core
Periphery
D
Glc (mM)
25
5
1
Colony number
500
400
300
200
100
0
wt
S473A
S473D
MDA-MB-231/shKAP1

Fig. 4

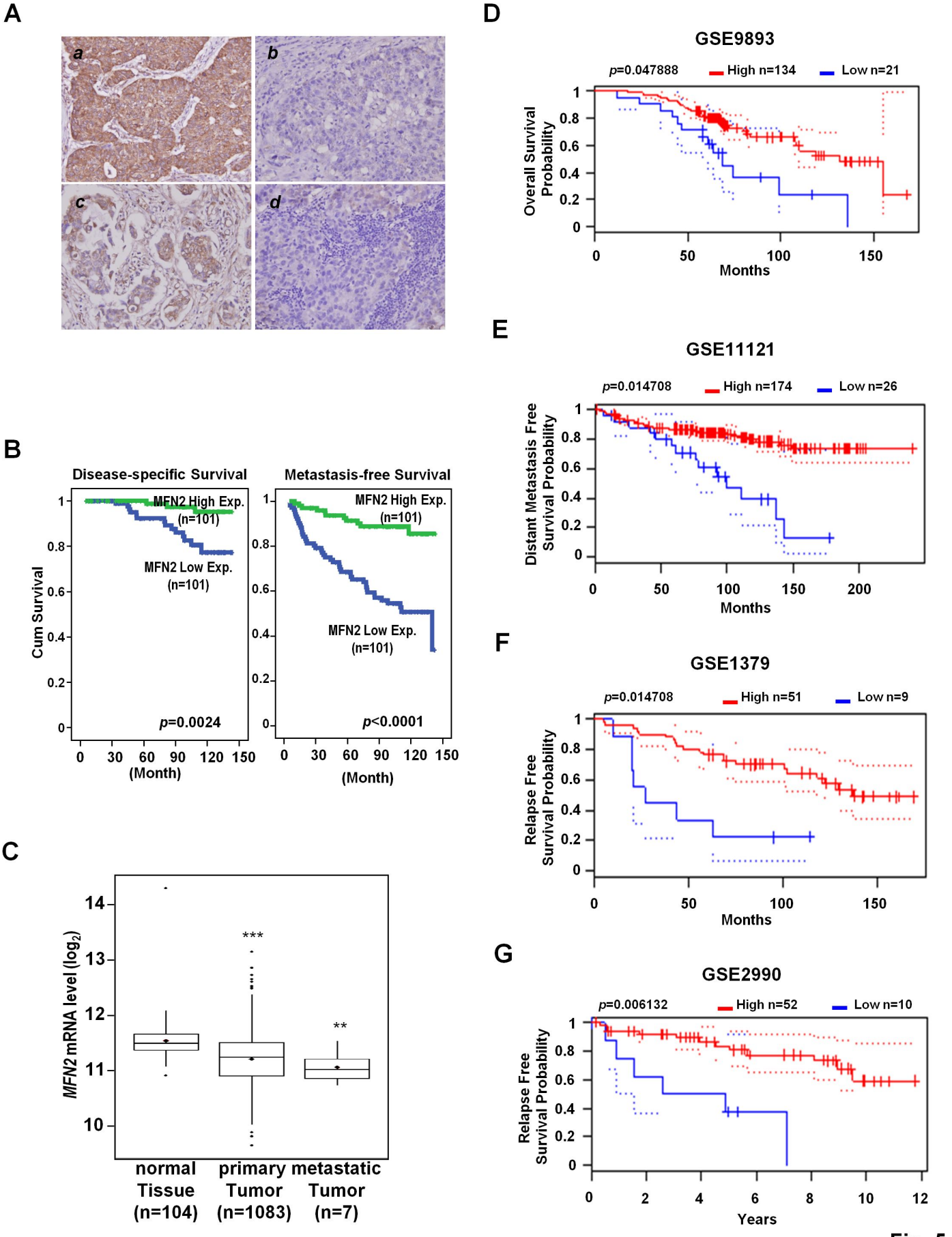
A
a
b
c
d
B
Disease-specific Survival
Metastasis-free Survival
MFN2 High Exp. (n=101)
MFN2 Low Exp. (n=101)
Cum Survival
p=0.0024
p<0.0001
(Month)
C
MFN2 mRNA level (log2)
***
**
normal Tissue (n=104)
primary Tumor (n=1083)
metastatic Tumor (n=7)
D
GSE9893
p=0.047888
High n=134
Low n=21
Overall Survival Probability
Months
E
GSE11121
p=0.014708
High n=174
Low n=26
Distant Metastasis Free Survival Probability
Months
F
GSE1379
p=0.014708
High n=51
Low n=9
Relapse Free Survival Probability
Months
G
GSE2990
p=0.006132
High n=52
Low n=10
Relapse Free Survival Probability
Years

Fig. 5

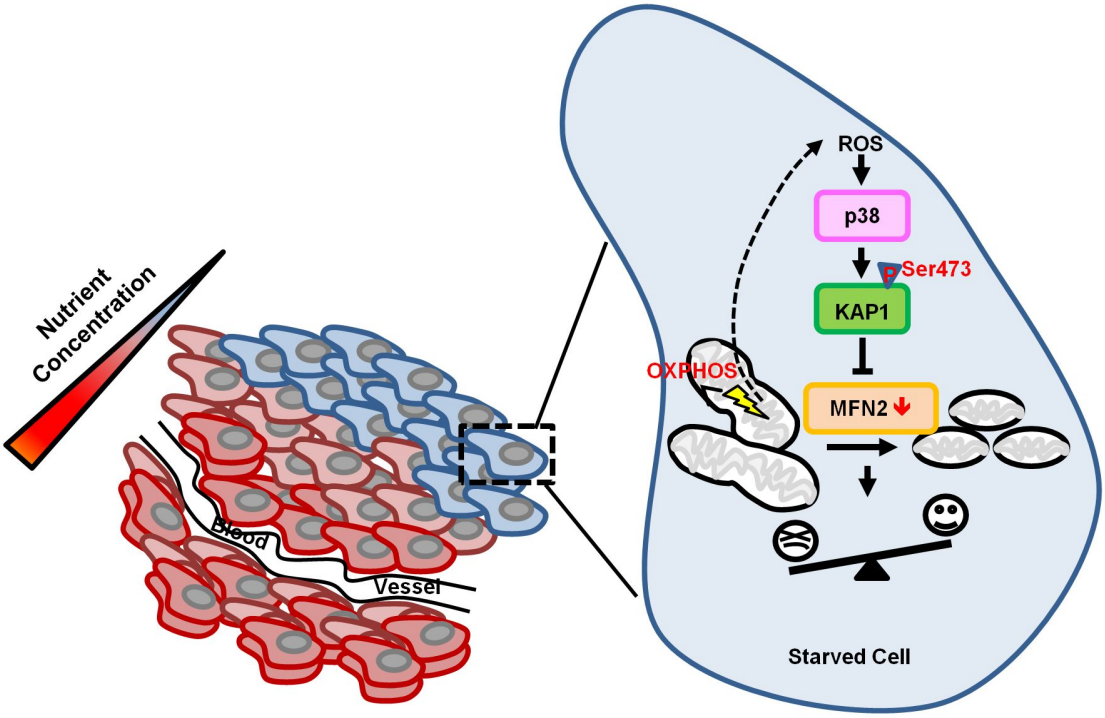
Nutrient Concentration
Blood
Vessel
ROS
p38
pSer473
KAP1
OXPHOS
MFN2
Starved Cell

Fig. 6